

Higher order variability properties of accreting black holes

Thomas J. Maccarone

Scuola Internazionale Superiore di Studi Avanzati, via Beirut, n. 2-4, Trieste, Italy, 34014

Paolo S. Coppi

Department of Astronomy, Yale University, P.O. Box 208101, New Haven CT USA 06520-8101

ABSTRACT

To better constrain the emission mechanism underlying the hard state of galactic black hole candidates, we use high-time resolution RXTE lightcurves for Cyg X-1 and GX 339-4 to compute two higher order variability statistics for these objects, the skewness and the Fourier bispectrum. Similar analyses, in particular using the skewness measure, have been attempted before, but the photon collection area of RXTE allows us to present results of much greater statistical significance. The results for the two objects are qualitatively similar, reinforcing the idea that the same basic mechanisms are at work in both. We find a significantly positive skewness for variability timescales less than ~ 1 second, and a *negative* skewness for timescales from 1 – 5 sec. Such a skewness pattern cannot be reproduced by the simplest shot variability models where individual shots have a fixed profile and intensity and are uncorrelated in time. Further evidence against simple shot models comes from the significant detection of a non-zero bicoherence for Fourier periods $\sim 0.1 - 10$ sec, implying that significant coupling does exist between variations on these timescales. We discuss how current popular models for variability in black hole systems can be modified to match these observations. Using simulated light curves, we suggest that the most likely way to reproduce this observed behavior is to have the variability come in groups of many shots, with the number of shots per unit time fitting an envelope function which has a rapid rise and slow decay, while the individual shots have a slow rise and a rapid decay. Invoking a finite energy reservoir that is depleted by each shot is a natural way of producing the required shot correlations.

Key words: accretion, accretion disks – methods:statistical – X-rays:binaries – X-rays:individual:Cygnus X-1 – X-rays:individual:GX 339-4

1 INTRODUCTION

The continuum X-ray and γ -ray spectra of accreting black holes generally consist of a soft component that can be described as a multi-colored black body and a hard component that can be well fit by a cutoff power law with some additional flux due to Compton reflection (see e.g. Zdziarski et al. 1997; Gierlinski et al. 1997; Poutanen 1998). Thermal Comptonisation models (with an additional non-thermal component sometimes required) provide a physical basis for producing such a spectrum. A variety of models with differing geometries can fit the spectral data (see e.g. Poutanen 1998; Beloborodov 1999; Zdziarski 2000), so one must find a means of breaking the spectral degeneracies in order to differentiate between possible geometries of the flow and mechanisms for producing the high energy electrons that upscatter photons into the hard tail of the spectrum.

Another useful characteristic of accreting black holes, especially those in hard spectral states, is rapid variability (see e.g. Nolan et al. 1981; Negoro, Miyamoto & Kitamoto 1994; Vaughan & Nowak 1997). Several variability properties of their lightcurve have already been studied extensively, especially for Cygnus X-1, and place constraints on the underlying emission mechanism. For example, Fourier spectra and cross-spectra have been used to show that the spectral energy distributions of Cygnus X-1 and GX 339-4 (the two canonical persistent black hole candidates in the Milky Way) cannot be produced by Compton scattering in a static, uniformly dense cloud of hot electrons (Miyamoto et al. 1988), as had been previously suggested (Payne 1980). The improved photon statistics that are now possible with large area detectors like the Rossi X-ray Timing Explorer (RXTE) merit a re-examination of some of these prior analyses.

In a previous paper, we presented measurements of the

cross-correlation function and autocorrelation functions of Cygnus X-1 at different energies which rule out all models in which the time lags between energy bands come from diffusion timescales through the corona. We also found that the autocorrelation and cross-correlation functions imply that the shape of individual shots in the hard state of Cygnus X-1 is such that the count rates rise more or less exponentially, then decay much more rapidly (Maccarone, Coppi & Poutanen 2000), the inverse of the FRED (fast-rise, exponential decay) behavior often cited in γ -ray burst studies (see e.g. Fenimore, Madras & Nayakshin 1996). This possibility can be evaluated and understood further by using the time skewness statistic, which measures the symmetry of a lightcurve as a function of time scale. Previous time skewness analyses showed that the light curve of Cygnus X-1 cannot be produced by purely exponential shots with either a rising or falling profile (Priedhorsky et al. 1979), but in our knowledge, this technique has not been applied since, despite immense advances in temporal resolution, photon statistics, and duration of observations. Here we present the results of time skewness analyses of RXTE data sets from Cygnus X-1 and GX 339-4 in their hard states. To complement this analysis, we also compute the Fourier bispectrum of the lightcurve data. The Fourier bispectrum (e.g. Mendel 1991) has been applied the spatial properties of the cosmic microwave background and large-scale structure (e.g. Cooray 2001) and to problems in other fields such as neurobiology (e.g. Bullock et al. 1995) and speech recognition (Fackrell 1996), but it has not previously been applied to astronomical time series data. With good quality data, however, we find that it provides another useful, higher order variability probe, determining whether the fluctuations on one time scale are coupled to the fluctuations on other timescales.

In section 2 we briefly describe the data set used and the data reduction and screening. In section 3, we define the statistics we use and present the observational results. In section 4, we discuss the mathematical form of the light curve implied by the observational results and consider the possible physical models that could produce the observed variability.

2 OBSERVATIONS

2.1 Reduction

Because of the need for large photon numbers to compute higher order variability statistics, we analyze the RXTE hard state data for the two brightest quasi-persistent low/hard state sources, Cyg X-1 and GX 339-4. The observations used are listed in Table 1. Light curves are extracted from the Proportional Counter Array (PCA) data in several different energy bands using the standard RXTE screening criteria of earth elevation greater than 10 degrees, pointing offset less than 0.01 degrees, having all 5 proportional counter units on, and having the standard amounts of time before and after South Atlantic Anomaly passages. In all cases, the time skewness is computed on a 0.125 second time scale. The photon statistics do not permit a computation on shorter timescales.

3 ANALYSIS

3.1 Time Skewness

3.1.1 Definition

The time skewness measures the asymmetry of a lightcurve. We choose a slightly different definition than Priedhorsky et al. (1979) in order to non-dimensionalise the skewness and to make the normalisation independent of constant scaling factor changes to the count rate:

$$TS(\tau) = \frac{1}{\sigma^3} [(s_i - \bar{s})^2 (s_{i-u} - \bar{s}) - (s_i - \bar{s})(s_{i-u} - \bar{s})^2], \quad (1)$$

where τ is defined to be u times the time bin size, s_i is count rate for the i th element of the light curve, and σ is the standard deviation of the count rate. Essentially, the time skewness is a weighted average of the difference between two count rates measured at a given separation in time. If a light curve is composed of the summation of spikes, and the spikes typically rise more sharply than they fall on a particular time scale, the sign of the skewness will be negative; if the spikes fall more sharply than they rise, the skewness will be positive. We compute the time skewness for each observation separately, then present the weighted average of the individual measurements. The errors plotted are the rms variations of the individual measurements used in the averaging, and may be overestimated if there is intrinsic variation in the time skewness.

3.1.2 Results

Throughout the rest of this paper the term ‘‘shot’’ will be used to describe a temporary increase in luminosity. In some cases in the literature this term has been used to describe models where the lightcurve consists of the random superposition of events with a single profile, duration, and intensity. Except when explicitly stated to have this meaning, we intend a more general definition of the word, and by referring to ‘‘shots’’, we may imply a distribution of flare shapes and durations. Additionally, the term ‘‘rising shot’’ will be used to describe a shot whose duration is dominated by its rise time, and the term ‘‘falling shot’’ will be used to describe a shot whose duration is dominated by its decay time.

The 2-5 keV (channels 0-13 in the PCA) skewnesses from Cygnus X-1 and GX 339-4 in their hard states are presented in Figure 1. Both objects have a strongly positive skewness out to about 1 second and a strongly negative skewness between 1 second and the time scale on which their autocorrelation functions go to zero (5 seconds for Cygnus X-1 and 3 seconds for GX339-4). Beyond the autocorrelation function decay time scale, their skewnesses are consistent with zero. Whether these characteristics apply to all objects’ hard states is difficult to determine, because the other persistent hard state sources are much fainter than Cyg X-1 and GX 339-4. Furthermore, the transient hard state sources often show strong, relatively narrow QPOs in their hard states which complicate this analysis.

The skewnesses for other energy bands were also computed and are presented in Figure 2, with the error bars removed to make the figure more clear. In Cygnus X-1, the skewnesses are identical within the errors across energy bands. There seems to be some indication for a more sym-

Table 1. The data analyzed for this the time skewness analyses. Dates are presented in DD/MM/YY format.

ObsID	Start Time	Stop Time	Source
30158-01-01-00	10/12/97 07:07:53	10/12/97 08:30:14	Cyg X-1
30158-01-02-00	11/12/97 07:06:14	11/12/97 08:45:14	Cyg X-1
30158-01-03-00	14/12/97 08:48:14	14/12/97 10:20:14	Cyg X-1
30158-01-04-00	15/12/97 03:49:42	15/12/97 05:26:14	Cyg X-1
30158-01-05-00	15/12/97 05:26:14	15/12/97 07:09:14	Cyg X-1
30158-01-06-00	17/12/97 00:39:55	17/12/97 02:05:14	Cyg X-1
30158-01-07-00	20/12/97 07:11:18	20/12/97 08:29:14	Cyg X-1
30158-01-08-00	21/12/97 05:28:14	21/12/97 07:05:14	Cyg X-1
30158-01-09-00	24/12/97 23:03:14	24/12/97 00:39:14	Cyg X-1
30158-01-10-00	25/12/97 00:39:14	25/12/97 01:45:14	Cyg X-1
30158-01-11-00	30/12/97 02:18:03	30/12/97 03:52:14	Cyg X-1
30158-01-12-00	30/12/97 03:52:14	30/12/97 05:30:14	Cyg X-1
20181-01-01-01	03/02/97 15:56:24	03/02/97 19:09:13	GX 339-4
20181-01-01-00	03/02/97 22:27:01	04/02/97 01:36:13	GX 339-4
20181-01-02-00	10/02/97 15:49:19	10/02/97 20:51:13	GX 339-4
20181-01-03-00	17/02/97 18:28:38	18/02/97 00:12:13	GX 339-4
20183-01-01-00	08/02/97 14:20:30	08/02/97 20:48:13	GX 339-4
20183-01-02-00	14/02/97 00:09:12	14/02/97 06:43:13	GX 339-4
20183-01-02-01	14/02/97 14:20:45	14/02/97 21:22:13	GX 339-4
20183-01-03-00	22/10/97 03:00:35	22/10/97 05:52:14	GX 339-4
20183-01-04-00	25/10/97 03:22:40	25/10/97 06:16:14	GX 339-4
20183-01-05-00	28/10/97 18:07:56	28/10/97 22:13:14	GX 339-4
20183-01-06-00	31/10/97 19:40:12	31/10/97 22:10:14	GX 339-4
20183-01-07-00	03/11/97 20:35:02	03/11/97 23:48:14	GX 339-4

Table 2. The data analyzed for the bicoherence analyses. Dates are presented in DD/MM/YY format.

ObsID	Start Time	Stop Time	Source
30158-01-01-00	10/12/97 07:07:53	10/12/97 08:30:14	Cyg X-1
30158-01-02-00	11/12/97 07:06:14	11/12/97 08:45:14	Cyg X-1
30158-01-03-00	14/12/97 08:48:14	14/12/97 10:20:14	Cyg X-1
30158-01-04-00	15/12/97 03:49:42	15/12/97 05:26:14	Cyg X-1
30158-01-05-00	15/12/97 05:26:14	15/12/97 07:09:14	Cyg X-1
30158-01-06-00	17/12/97 00:39:55	17/12/97 02:05:14	Cyg X-1
30158-01-07-00	20/12/97 07:11:18	20/12/97 08:29:14	Cyg X-1
30158-01-08-00	21/12/97 05:28:14	21/12/97 07:05:14	Cyg X-1
30158-01-09-00	24/12/97 23:03:14	24/12/97 00:39:14	Cyg X-1
30158-01-10-00	25/12/97 00:39:14	25/12/97 01:45:14	Cyg X-1
30158-01-11-00	30/12/97 02:18:03	30/12/97 03:52:14	Cyg X-1
30158-01-12-00	30/12/97 03:52:14	30/12/97 05:30:14	Cyg X-1
20056-01-01-00	05/04/97 08:36:14	05/04/97 09:15:13	GX 339-4
20056-01-02-00	10/04/97 11:47:29	10/04/97 12:28:13	GX 339-4
20056-01-03-00	11/04/97 13:25:44	11/04/97 14:06:13	GX 339-4
20056-01-04-00	13/04/97 20:09:51	13/04/97 20:50:13	GX 339-4
20056-01-05-00	15/04/97 20:41:10	15/04/97 21:23:13	GX 339-4
20056-01-06-00	17/04/97 23:25:47	18/04/97 00:01:13	GX 339-4
20056-01-06-01	18/04/97 00:01:13	18/04/97 00:09:13	GX 339-4
20056-01-07-00	19/04/97 22:20:01	19/04/97 23:21:13	GX 339-4
20056-01-08-00	22/04/97 21:53:21	22/04/97 22:29:13	GX 339-4

metric overall lightcurve (i.e. a lower amplitude of the skewness) on long timescales in the higher energy bands, but it is not clear whether this is a real effect or due to the lower count rates at higher energy introducing more Poisson noise. In GX 339-4, the skewnesses become more symmetric as a function of increasing energy. This agrees well with the observation that the Fourier spectrum in GX 339-4 is consistent with being constant as a function of energy, while the Fourier time lags become longer for larger energy separations (e.g. Lin et al. 2000). We note that the large difference between the 15-45 keV lightcurve's skewness and the

lower energy bands' skewnesses is due to the effects of Poisson noise artificially increasing the variance which is used to normalise the skewness values. This cannot be the case for the two lower energy bands, since the intermediate band has a count rate about 10% *higher* than the lowest energy band, and still has a lower skewness. Still the differences in the skewness as a function of energy are not particularly large, and it would be worthwhile to re-investigate this effect with the entire RXTE data set for GX 339-4 at the end of the mission.

The combination of the skewness measurements and the

previous power spectrum results suggests that as the energy band increases, the rise timescale of a shot becomes slightly shorter while its decay timescale becomes somewhat longer. Thus the shots in GX 339-4 become more symmetric at higher energies and the normalisation of the skewness becomes smaller. Previous results found only that one-sided exponential shot models could be ruled out, and did not look to long enough timescales to see the sign change in the skewness (Priedhorsky et al. 1979). The fluctuations in the amplitude of the negative peak are of order the fluctuations in the skewness on 5-10 second timescales where the mean observed and expected values are ~ 0 . We thus do not ascribe any physical meaning to the observed fluctuations in the skewness within the peak.

The statistical properties of the time skewness are not well established. In order to ensure that our results are not due to measurement errors, we create simulated data sets of time-symmetric red noise with the phases at different frequencies uncorrelated with one another, using the algorithm of Timmer & König (1995), with a power spectral form similar to the observed power spectrum of Cygnus X-1 (a constant value below 0.1 Hz joined continuously to a f^{-1} power law from 0.1 to 1 Hz and then to a $f^{-1.7}$ power law above 1 Hz, with an rms amplitude of 30%). One hundred lightcurves are simulated, each with a duration of 10 kiloseconds (shorter than the 30 kilosecond integration used in the Cygnus X-1 data set, which means that the real computation should be more robust than the simulated data computation). None of the simulated light curves show skewnesses on time scales of less than 1 second that could match the first peak (i.e. with absolute values greater than 0.02, the magnitude of the first peak). While three of the lightcurves show a skewness in the 2-4 second range with an absolute value of at least 0.04 (the size of the negative peak), there are no lightcurves with absolute values greater than 0.02 for the entire 2-4 second region, as is seen in Cygnus X-1. The mean value in the 2-4 second range is about 0.01, which are about the same size as the errors plotted in Figure 1. Thus, individual time bins from random light curves may occasionally (but infrequently) show skewnesses as large as the observed one, but they do not produce broad peaks in the skewness with depths as large as the observed depths. The randomly generated lightcurves do frequently have skewnesses half the size of those observed. This underscores the importance of long integrations for making skewness measurements, even when the photon statistics are good, since a short lightcurve, even with perfect photon statistics, can produce large skewness values despite having random Fourier phases at all frequencies.

The power spectrum for GX 339-4 is roughly the same as for Cygnus X-1, except that the high frequency cutoff occurs at about 3 Hz rather than 1 Hz. We simulate 40 kilosecond lightcurves (our observations are 46 kiloseconds here) with the power spectral shape for GX 339-4. As the observed skewness for GX 339-4 has a broad trough from 3 to 5 seconds at -0.015, we look for observations where the skewness has an absolute value of at least 0.015 over the entire 3 to 5 second range. We find no such lightcurves out of our 100 simulated lightcurves, and find only 3 lightcurves with any points with absolute values greater than 0.015 for any bin from 3 to 5 seconds. Thus again we find that while rarely, but occasionally, the depths of the troughs can be matched by

the red noise lightcurves, troughs with the necessary depth and breadth cannot.

3.1.3 Other spectral states

The time skewnesses were also computed for Cygnus X-1 in its transition state and in its soft state and for LMC X-1 which appears to have only a soft state. Since the rms variability amplitudes in the softer states are typically much lower than in the hard states (making variability harder to measure), and the characteristic variability time scales are shorter (making binning the data up to longer time scales problematic), the skewnesses computed were very noisy, and it was difficult to draw any useful conclusions from them. Thus we neither plot nor discuss these results.

3.2 Fourier bispectrum

3.2.1 Definition

The bispectrum computed from a time series broken into K segments is defined as:

$$B(k, l) = \frac{1}{K} \sum_{i=0}^{K-1} X_i(k) X_i(l) X_i^*(k+l), \quad (2)$$

where $X_i(k)$ is the frequency k component of the discrete Fourier transform of the i th time series (e.g. Mendel 1991; Fackrell 1996 and references within). It is a complex quantity that measures the magnitude and the phase of the correlation between the phases of a signal at different Fourier frequencies. Its value is unaffected by additive Gaussian noise, although its variance will increase for a noisy signal.

A related quantity, the bicoherence is the vector magnitude of the bispectrum, normalised to lie between 0 and 1. Defined analogously to the coherence function (e.g. Nowak & Vaughan 1996), it is the vector sum of a series of bispectrum measurements divided by the sum of the magnitudes of the individual measurements. If the biphas (the phase of the bispectrum) remains constant over time, then the bicoherence will have a value of unity, while if the phase is random, then the bicoherence will approach zero in the limit of an infinite number of measurements. The bicoherence is defined as:

$$b^2(k, l) = \frac{|\sum X_i(k) X_i(l) X_i^*(k+l)|^2}{\sum |X_i(k) X_i(l)|^2 \sum |X_i(k+l)|^2}. \quad (3)$$

This analysis will concentrate on the bicoherence, since statistically significant measurements of it are easier to make. The denominator of this expression has a dependence on the amount of Gaussian noise, so a correction will have to be made when the signal is noisy. Additionally, the bicoherence, being bound between 0 and 1, has a non-zero mean value due to errors even when the phases of the Fourier transforms are uncorrelated. The mean value and the standard deviation of a bicoherence estimate based on K distinct Fourier transforms are both $\frac{1}{K}$. The properties of the bispectrum and the bicoherence as they relate to time series analysis are well-reviewed by Fackrell (1996).

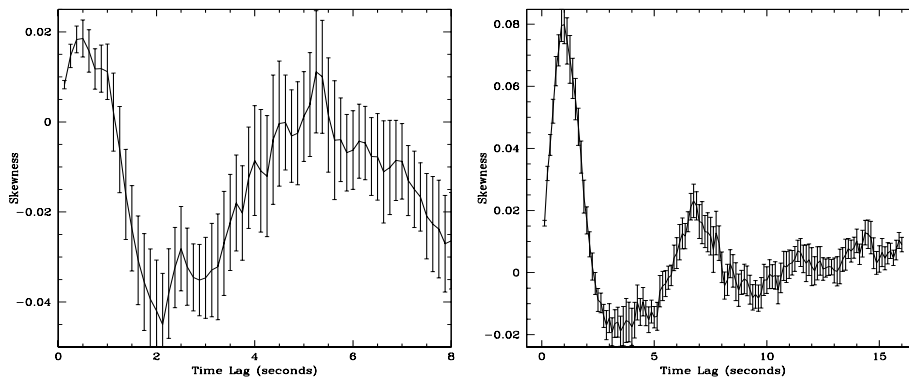


Figure 1. The 2-5 keV skewnesses for (a) the hard state of Cygnus X-1 and (b) the hard state of GX 339-4.

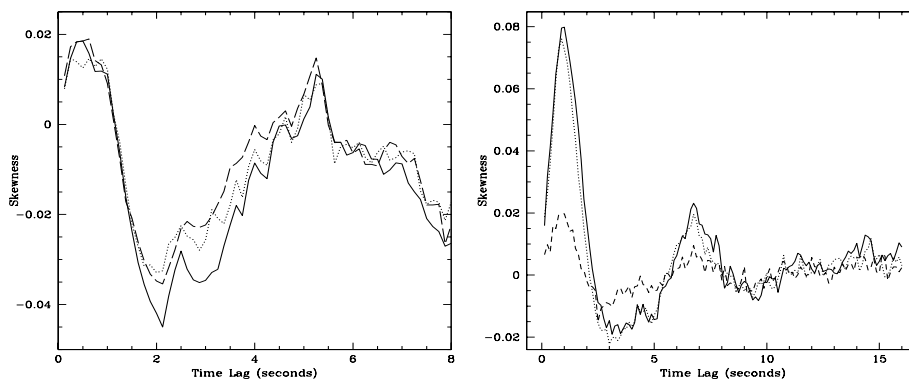


Figure 2. The higher energy band skewnesses, plotted without error bars for (a) Cygnus X-1 in the hard state (solid line is 2-5 keV, dotted line is 5-7 keV and dashed line is 7-10 keV) and (b) GX 339-4 in the hard state (solid line is 2-5 keV, dotted line is 5-15 keV, and the dashed line is 15-45 keV).

3.2.2 Computation method and results

The lightcurves are split into segments of 4096 elements (since the time resolution of the lightcurves varies, the lengths of these segments in absolute amounts of time will also vary). Fourier transforms are computed for each element. The results are then combined according to equation (2) to estimate the bicoherence. The data used to compute the bispectra are listed in Table 2.

Since the bicoherence is a function of two independent variables, one could presumably gain the most information from a 3 dimensional plot, or a two dimensional contour plot. Since we find from inspection that, for these data, no individual peaks stand out in such plots, the data are rebinned to present the results only as a function of the sum of the

two lower Fourier frequencies. This allows for a simple two-dimensional plot, allows for significant data rebinning to increase the statistical significance of the results, and does not remove any obvious underlying trends. Similar techniques are frequently used in analyses of spatial bispectra of the microwave background, although in that case the computations are done in terms of spherical harmonics rather than Fourier frequencies. We caution the reader who may wish to try this technique on other time series that for systems with strong, relatively narrow quasi-periodic oscillations, rebinning the frequencies to one dimension may result in the loss of important signals. For example, we have examined a few observations of GRS 1915+105 where the 1-10 Hz QPOs show harmonic structure and have found that the bicoherence can be quite strong for the pairs of frequencies that

add up to the frequencies of the higher harmonics, but that this effect can be seen clearly only from a three dimensional plot.

We have plotted the results for the bicoherence measurements for Cygnus X-1 (from 2-5 keV; channels 0 to 13) and GX 339-4 (from 2 to 8 keV; channels 0 to 25) in Figures 3 (a) and (b) respectively. In all cases, the bispectrum fits a broken power law with a negative index for high frequencies; for lower frequencies, it has a nearly constant value. The non-zero bicoherence indicates that the variability at low frequencies is coupled to the noise at high frequencies, providing an additional piece of strong evidence that a single shot model cannot match the data. Furthermore the phases of the Fourier components are more strongly correlated at low frequency than they are at high frequency.

We attempted similar analyses for data from accreting neutron stars, but the photon statistics were not sufficient to find interesting results. There is not sufficient RXTE data on any single neutron star in the island state of an atoll source (the analog of the hard state for black hole sources) to make use of this technique. Likewise, LMC X-1 (the most variable and best observed soft state source) lacks sufficient signal to noise to make use of the bispectrum. For objects with strong quasi-periodic oscillations, the analysis is significantly more complicated, as some frequencies may represent the harmonics of periodicities found at lower frequencies. Such analysis is outside the scope of this paper which aims merely to characterise random noise components of the power spectra of accreting objects.

4 DISCUSSION

We now consider possible models and attempt to determine how they match the key observational results - that (1) the skewness is positive on short timescales, (2) the skewness changes sign and becomes negative on timescales of about 1 to 5 seconds before going to zero on long timescales and (3) that the bicoherence has a “shelf” at low bifrequency. We also will make use of the result of Priedhorsky et al. (1979), reproduced here, that the normalisation of the skewness found in the data is much smaller than the normalisation of the skewness found from a one-sided exponential shot distribution. An exact reproduction of the time skewness is likely to be a quite complicated problem numerically, as the shot shapes and arrival times may take non-standard functional forms. We first discuss toy models that approximate the mathematical form of the skewness then discuss recent theoretical models which might be expected to produce this mathematical form. Finally, we show that the bicoherence results agree with the general mathematical form used to match the skewness, providing an independent confirmation of our picture. In the models we consider, we invoke the “shot noise” hypothesis - that the variability consists of discrete events. Our conclusions that the lightcurve shows a different sense of asymmetry on different timescales are independent of this assumption. The specific interpretations below are not so clearly robust.

One possible means of producing a skewness function which has both positive and negative signs is to create a light curve which has both rising and falling shots, with different time scales for the rising shots than for the falling

ones. This would seem to imply two physical mechanisms for producing shots. Furthermore, to produce hard lags on all time scales from this distribution, as is required from the Fourier cross spectrum, one would need the rising shots to be shorter with increasing energy while the falling shots would have to be longer with increasing energy. This would produce an autocorrelation function that becomes wider with increasing energy on long time scales, in violation of observational constraints. We were unable to find a distribution of shot intensities and time scales for this scenario that reproduced the observed skewness.

A second model one might consider would be to have a random superposition of identical two-sided shots, with a rise time different from the fall time. Two sided shots, however, fail to reproduce to observed skewness measurements. They are always dominated by the longer timescale, and actually fail to produce skewnesses which have both substantial positive and negative portions on different time scales.

A third possibility is to have all the shots be rising exponentials with sharp cutoffs (inverse FREDs), while the probability of having a shot occur at a given time is given by an exponentially falling function (an actual FRED, i.e., the mean shot rate is proportional to $\lambda \propto \exp[-(t - t_0)/\tau]$ for $(t > t_0)$). Thus the rising shots are embedded in a falling envelope. In this paper, the envelopes will be modeled by drawing the arrival times of the peaks of the shots from an exponential deviate; more complicated envelope functions are possible but are not considered here. Figure 4(a) illustrates the difference between rising and falling shots, while Figure 4(b) shows rising shots embedded in a falling envelope.

An “envelope” model with one-sided exponential rising shots with a rise time of 0.5 seconds and a one-sided exponential envelope with a decay time of 4 seconds matches the qualitative trends of the observed skewness, but the overall normalisations of the skewness are a factor of ~ 10 too large, indicating that this model assumes much more asymmetry than is present in nature. We thus modify the model by giving both the envelope and the shots two-sided profiles. The resulting model lightcurve has a skewness that matches the observations within factors of a few. For the time scales on which the individual shots occur, the skewness is positive. For time lags of duration between the individual shot time scale and the “envelope” time scale, the skewness is negative. For time lags longer than the envelope scale, the skewness is zero. Skewness computations for a simulation with shots having an 0.5 second rise time scale and an 0.1 second decay time scale embedded in an envelope with a 2.7 second rise time scale, a 3.0 second decay time scale and 53% of the shots in the decaying portion (so that the rising and decaying portions of the envelope will form a continuous function) are computed. Each model lightcurve contains 25 shots. Since the process is random, 149 lightcurves have been computed and the results have been averaged to improve the statistics. The simulated skewness for this model is plotted in Figure 5 (a) and a sample simulated lightcurve is plotted in Figure 5 (b). We have also computed the skewness of a simulated lightcurve made of a random superposition of the 25 shot lightcurves. We find that the smearing of the shots induced by this superposition does not affect the results substantially. In order to fit the skewnesses more exactly, one

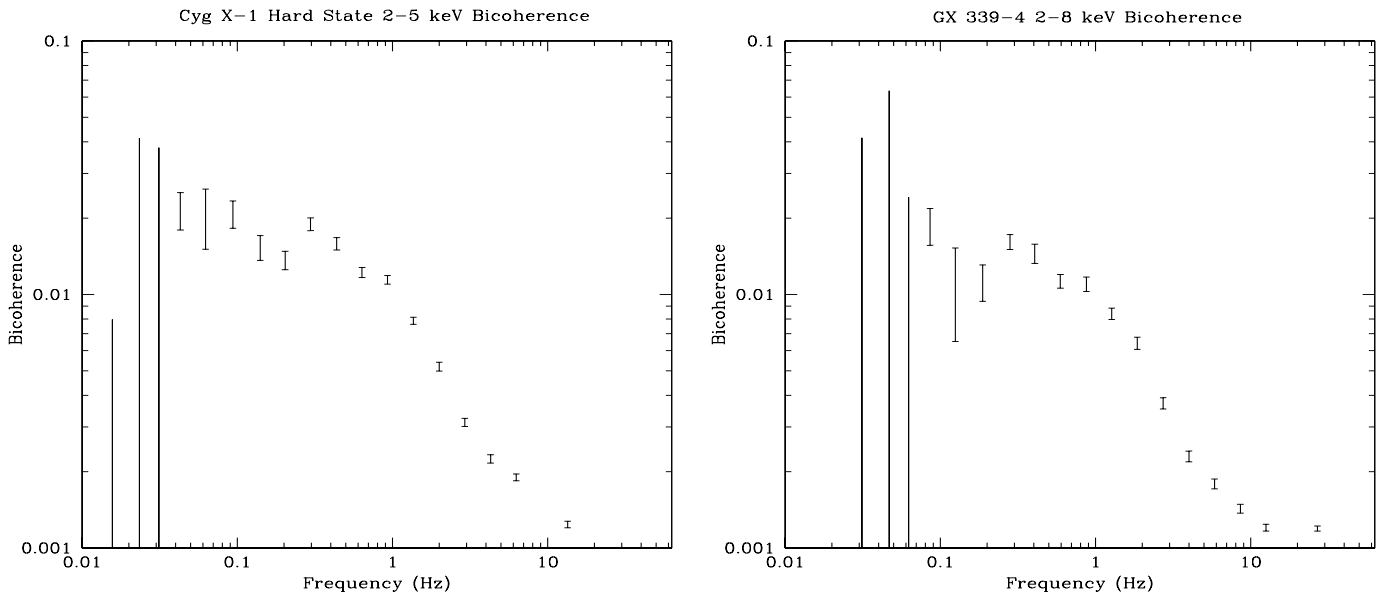


Figure 3. The bicoherence plots for (a) Cyg X-1 and (b) GX 339-4 in the hard state.

needs to modify the parameters of the simulation by varying the ratios of rise time to decay time. A model in which the shot and envelope time scales are allowed to vary with some small range around an average produces essentially the same skewness results as the single time scale models, and if the number of shots per unit time is too high, then the individual shots blend together so much that the skewness reflects only the envelope. The idea that the shots cannot be independent stochastic events was also suggested by Uttley & McHardy (2001) to explain the constancy of RMS variability as a function of count rate in Cyg X-1, SAX J1808.4-3658, and several Seyfert galaxies.

A final possibility is related to the third one. One can have the shot arrival times be independent of one another, while their intensities are correlated with one another. If large shots are followed only by smaller shots, then the general form of the skewness can be reproduced.

Such a mathematical form can be reproduced by two recent models - the self-organised criticality (SOC) model (Takeuchi, Mineshige & Negoro, 1995; Takeuchi & Mineshige 1997) and the pulse avalanche model (Poutanen & Fabian 1999). The skewness of a simulated light curve that borrows the major results of the SOC model is presented in Figure 6a, and a segment of the simulated light curve is plotted in Figure 6b. In this simulation, an energy reservoir is posited and shot arrival times are presumed to be random. Each shot results in the release of a random fraction of the energy reservoir. The duration of the shot is related to the energy released at $\tau \propto E^{0.4}$. The energy reservoir is refilled at a constant rate. Thus when a large shot occurs, the reser-

voir's energy level will be depleted and subsequent shots will be smaller until the reservoir is re-filled. The shots are given Lorentzian profiles and their τ values are given by the ratio of the reservoir's energy level to the mean reservoir energy level times a random value drawn from a uniform distribution between 0.05 and 0.15 seconds. A 1000 second simulated light curve is produced, allowing us to average over many reservoir-filling timescales.

Current applications of the SOC model to black hole binary light curves fail to match several well established observational constraints for Cygnus X-1 and GX 339-4. They assume a shot with the reverse time sense of those seen in the observations. This is not an essential component of the model since the shot profile is put in by hand to match the power spectrum, and our simulation has already changed this property of the shots and assumed the shots decay rapidly rather than rise rapidly. Additionally, this model does not attempt to explain the time lags seen in black hole binaries in the hard state. Both these problems could probably be solved, at least qualitatively, by assuming that the gas in a shot event gets hotter as it falls in, then abruptly stop emitting light when it reaches the event horizon of the black hole. This would result in a shot with a rising profile, a sharp turnoff, and hard lags.

More troubling is the inability of the ADAF/SOC model to match the observed luminosity. Because it assumes the standard parameters from Narayan & Yi (1995), the total amount of energy in electrons in the corona is small (of order 10^{34} to 10^{35} ergs), the accretion rate must be small, and the accretion flow must radiate inefficiently. This makes it

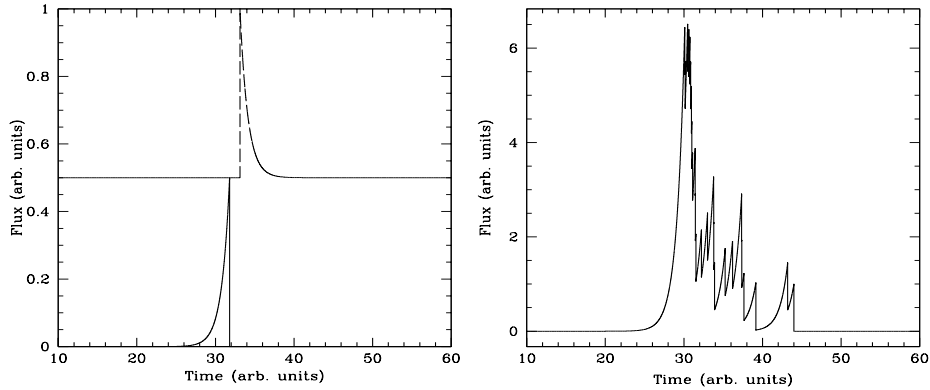


Figure 4. (a) A rising shot (solid line) and a falling shot (dashed line) (b) Rising shots imbedded in a falling envelope.

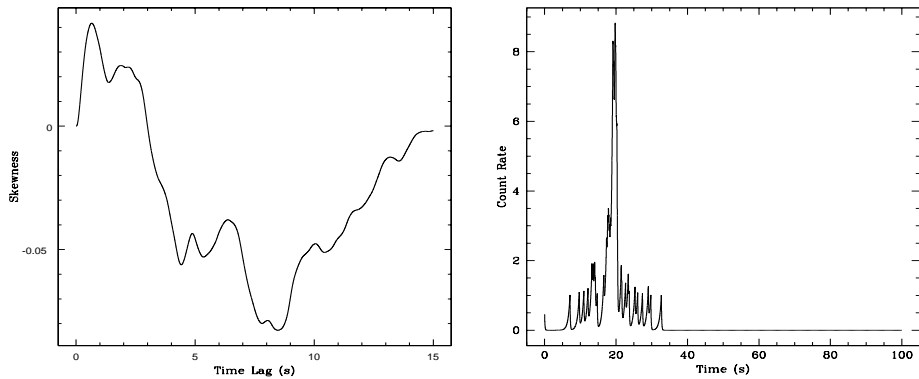


Figure 5. (a) The time skewness of a simulated lightcurve made of an envelope of shots where the envelope has an exponentially rising envelope with a 2.7 second time scale, an exponentially decaying envelope with a 3.0 second time scale and shots with 0.5 second rise time scales and 0.1 second decay time scales (b) a typical example of the lightcurve that produced this profile.

difficult to supply the required luminosity for Cygnus X-1 and GX 339-4 in their hard states, since the hard states of these sources are more luminous than those of most other accreting black hole candidates. Thus the models of Takeuchi & Mineshige (1998) predict a luminosity of only $\sim 10^{34}$ ergs/sec, while the luminosity of Cygnus X-1 in its hard state is about a factor of 1000 higher than that value.

Still, the skewness of the lightcurve is fairly well matched by the SOC model. This success may suggest that some conceptually similar process - an energy reservoir of

some sort drives the variability; when that reservoir is depleted, production of large shots is suppressed. We also note that a gradual mass flow in addition to the self-organized critical flow is required to produce an f^{-1} power spectrum rather than a steeper f^{-2} decay. Whether some form of the SOC model could reproduce the lightcurve of Cygnus X-1 given a set of coronal parameters which reproduces the spectrum more accurately (such as that of Esin et al. 1998) remains to be seen. *At the present, the problem is with the specific parameters used in the ADAF realisation of the SOC*

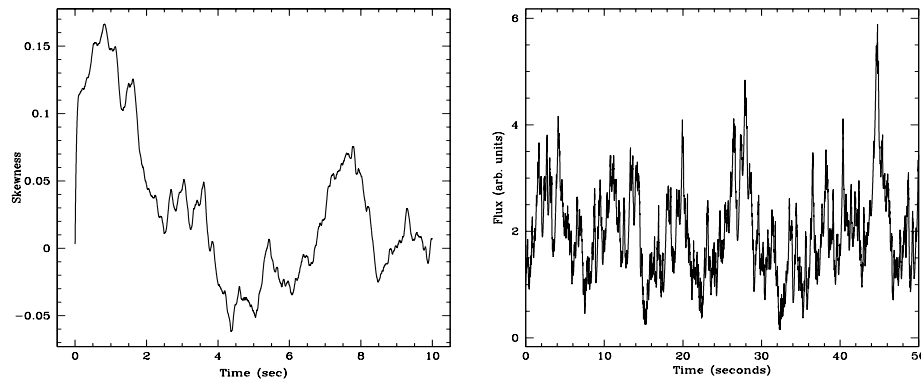


Figure 6. (a) The time skewness of a simulated lightcurve made from a model in which the size of a given shot is a random number times a fraction of the energy remaining in an energy reservoir. (b) The first 50 seconds of the simulated lightcurve in our reservoir model.

model and not with the SOC model itself. We note that our simulated “envelope” model has a similar problem of having its power spectrum fall off too rapidly at high frequencies. To fix the problem, a sharper than exponential envelope function would be needed.

The magnetic flaring model of Poutanen & Fabian (1999) is an alternative mechanism for producing the both the hard emission and the variability seen in low/hard state objects. This model produces the time lags through temperature changes in an active region. Each shot has a probability of causing another shot to occur and the mean delay time before the emission of the stimulated shot is proportional to the energy of the stimulating shot. The requirement that the magnetic energy reservoir be refilled before another shot occurs could be the cause of this delay. The possibility that a magnetic energy reservoir is required to heat the corona in accreting systems has been discussed recently (Merloni & Fabian 2001).

Another recent observational result that can perhaps be explained in terms of these multiple time scales, either due to reservoir effects or exponential envelopes of shots, is the decomposition of the Fourier power spectrum into multiple Lorentzian peaks (e.g. Nowak 2000). This approach typically yields between 3 and 7 peaks in the power spectrum, but the basic idea that the variability has multiple characteristic time scales is present in both our results and the “many-QPO” interpretations of the power spectra. The strongest peaks in the Fourier spectrum may correspond to the time scales presented here and the other peaks in the Fourier spectrum may be unresolvable with current skewness measurements or may require yet higher order moments of the light curve to be computed.

Finally, assuming that a shot-noise type model is correct, it is noted that in Cygnus X-1, these results present evidence for a significant constant (or quasi-constant) flux component. Since the shots have now been fairly clearly

demonstrated to be shorter at higher energies, the rms variability expected due to the shots should rise as a function of energy. But in the observations (e.g. Nowak et al. 1999), the rms decreases as a function of increasing energy. In order to reconcile these two observations, one must include an additional component with a significantly harder spectrum than that emitted by the shots, or we must assume that the shots have different properties at different energies (e.g. different relative amplitudes or different arrival frequencies). In the context of a shot model, the variable relative amplitude hypothesis would specifically require that the brightest shots would have softer spectra than the faintest ones, while the variable arrival frequency would require that some shots show up in the hard energy bands without contributing to the low energy bands. Given the observation that the coherence function is greater than 0.95 on all timescales from 0.01 Hz to 10 Hz, but drops significantly above 10 Hz (Nowak et al. 1999), the hypothesis that there are more shots at high energies than at low energies can be restricted to the case where the extra shots at high energies contribute almost no power on timescales longer than 0.1 seconds. While the near unity cross-correlation functions can be used to constrain how much the shots’ spectra can vary (Maccarone, Coppi & Poutanen 2000), rather large differences in shot spectra can be allowed as long as the peaks are aligned. Positing a constant component with a harder spectrum than the variable component would seem to contradict the results of Uttley & McHardy (2001) who found evidence for a constant component with nearly the same spectrum as the variable component. Thus it seems that the picture where the brightest shots have the softest spectrum is the most likely one. The possibility that the reflection component contributes to the drop in rms amplitude at the highest energies (those > 13 keV, which were not studied by Uttley & McHardy) remains viable.

Essentially the same implications are found from the

bicoherence measurements as from the time skewness measurements. We find that the $\sim f^{-1}$ dependence of the bicoherence function at high frequencies cannot be well matched by a single shot model. In Figure 7 we show the results from a model bicoherence computation for a simulated lightcurve with an envelope that rises instantaneously and decays exponentially on a timescale of four seconds, which is composed of shots that rise on an exponential timescale and decay instantaneously. The rise times of the shots are distributed uniformly between 0.5 and 1.5 seconds. The resulting bicoherence measurements are plotted in Figure 7, and match the observations reasonably well. Because of the computational intensity of bicoherence calculations and the uncertainties about whether the shot shapes should be exponentials, stretched exponentials, or some other more complicated profile, we cannot find an exact set of parameters for the shots and their envelopes.

5 SUMMARY

We have shown that the hard states of Cygnus X-1 and GX 339-4 have qualitatively similar skewness and bispectrum properties. They cannot be matched by any of the simplest single shot models. We suggest the possibility that either a model with a falling envelope of rising flares or a model with an energy reservoir that suppresses large shots following other large shots can reproduce the data, and that only models in which the arrival times and/or luminosities of the shots are correlated with one another can reproduce the skewness function which has both positive and negative parts. Whether the reservoir is one of accreting mass or of magnetic energy cannot be determined with the current data. Of the current variability models, the self organised criticality models or the magnetic flaring pulse avalanche models seem most likely to be able to fit this data without major modifications.

6 ACKNOWLEDGMENTS

We thank Rick Rothschild for pointing out that the time skewness could be used to test whether shots are symmetric and Roger Blandford for suggesting the use of the bispectrum to augment the skewness results. We are grateful to Phil Uttley for useful discussions regarding the constant component in Cygnus X-1. We thank the anonymous referee for making several useful suggestions. This research has made use of data obtained from the High Energy Astrophysics Science Archive Research Center (HEASARC), provided by NASA's Goddard Space Flight Center.

REFERENCES

Beloborodov, A.M., 1999a, in ASP Conf. Ser. 161, High Energy Processes in Accreting Black Holes, ed. J. Poutanen, R. Svensson (San Francisco: ASP), 295 (astro-ph/9901108)
 Bullock, T.H., Achimowicz, J.Z., Duckrow, R.B., Spencer, S.S. & Iragui-Madoz, V.J., 1995, EEG Clin. Neurophysiol., 103, 661
 Cooray, A., 2001, PhRvD, 64, 3516
 Esin, A.A., Narayan, R., Cui, W., Grove, J.E. & Zhang, S.N., 1998, ApJ, 505, 854

Fackrell, J., 1996, Ph.D. Thesis, University of Edinburgh
 Fenimore, E., Madras, C. & Nayakshin, S., 1996, ApJ, 473, 998
 Feng, Y.X., Li, T.P. & Chen, L., 1999, ApJ, 514, 373
 Gierlinski, M., Zdziarski, A.A., Done, C., Johnson, W.N., Ebisawa, K., Ueda, Y., Haardt, F. & Philips, B.F., 1997, MNRAS, 288, 958
 Lin, D., Smith, I.A., Böttcher, M. & Liang, E.P., 2000, ApJ, 531, 963
 Maccarone, T.J., Coppi, P.S. & Poutanen, J., 2000, ApJL, 537L, 107
 Merloni, A. & Fabian, A.C., 2001, MNRAS, 321, 549
 Mendel, J., 1991, Proceedings of the IEEE, 79, 278
 Miyamoto, S. & Kitamoto, S., 1989, Nature, 342, 773
 Narayan, R. & Yi, I., 1995, ApJ, 472, 710
 Nowak, M.A., 2000, MNRAS, 318, 361
 Nowak, M.A., Vaughan, B.A., Wilms, J., Dove, J.B. & Begelman, M.C., 1999, ApJ, 510, 874
 Negoro, H., Miyamoto, S. & Kitamoto, S., 1994, ApJL, 423, L127
 Payne, D.G., 1980, ApJ, 237, 951
 Poutanen, J. & Fabian, A. C. 1999, MNRAS, 306, L31
 Poutanen, J., 2000, in X-Ray Astronomy 1999: Stellar Endpoints, AGN, and the Diffuse X-Ray Background, in press (astro-ph/0002505)
 Priedhorsky, W., Garmire, G.P., Rothschild, R., Boldt, E., Serlemitsos, P. & Holt, S., 1979, ApJ, 233, 350
 Takeuchi, M. & Mineshige, S., 1997, ApJ, 486, 160
 Takeuchi, M., Mineshige, S. & Negoro, H., 1995, PASJ, 47, 617
 Timmer, J. & König, M., 1995, A&A, 300, 707
 Uttley, P. & McHardy, I.M., 2001, MNRAS, 323, L26
 Vaughan, B.A. & Nowak, M.A., 1997, ApJL, 474, 43L
 Zdziarski, A.A., Johnson, W.N., Poutanen, J., Magdziarz, P. & Gierlinski, M., 1997, in ESA SP-382, The Transparent Universe, Proc. of 2nd INTEGRAL workshop, ed. C. Winkler, T. J.-L. Courvoisier, Ph. Durochoux (Noordwijk: ESA), 373
 Zdziarski, A.A., 2000, in IAU Symp. 195, Highly Energetic Physical Processes and Mechanism for Emission from Astrophysical Plasmas, ed. P. Martens, S. Tsuruta, in press (astro-ph/0001078)

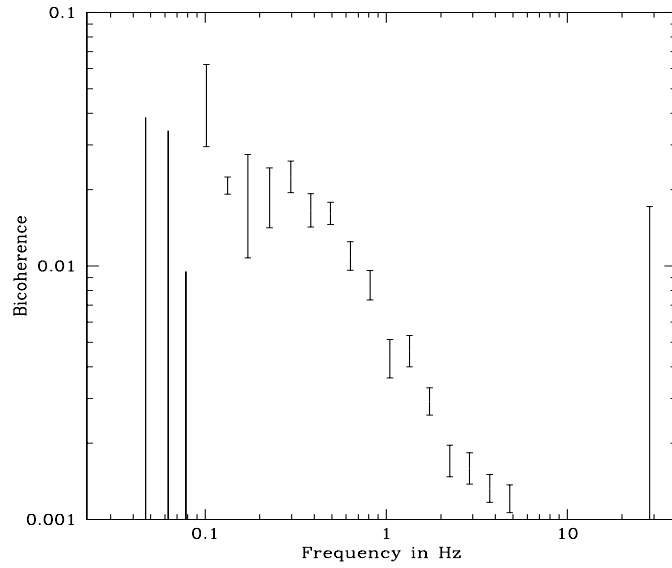


Figure 7. The bicoherence of a simulated light curve with a falling envelope of rising shots. The envelope's rise and decay times are 0 and 4 seconds respectively, while the shots' rise times are distributed randomly between 0.5 and 1.5 seconds and their decay times are instantaneous.